Int. J. Solids Structures, 1968, Vol. 4, pp. 741 to 756. Pergamon Press. Printed in Great Britain

DYNAMIC PLASTIC FLOW BUCKLING OF SHORT CYLINDRICAL SHELLS DUE TO IMPULSIVE LOADING*

ALEXANDER FLORENCE and HENRY VAUGHAN

Stanford Research Institute, Menlo Park, California

Abstract—A theory is postulated to explain the dynamic plastic buckling of short cylindrical shells subjected to uniform radially inward impulses. Formulas are derived which predict wavelengths (or mode numbers) and threshold impulses in general agreement with the experimental results that are presented. According to the theory, the restoring moment primarily consists of a directional moment brought about by yielding in a biaxial plastic state of stress; for the practical strain hardening values used the hardening contribution to the restoring moment is secondary. This conclusion is based on the relative influences on the preferred modes and threshold impulses.

INTRODUCTION

EXPERIMENTS carried out by Abrahamson and Goodier [1] demonstrate that cylindrical shells buckle plastically when subjected to sufficiently large uniform radially inward impulses. Each shell exhibited a predominant wavelength which was found to be reproducible. To account for the observed buckling they postulated a theory applicable to rigid–plastic materials in which buckling stems from imperfections in uniform initial velocities or displacements. The theory assumes that no strain-rate reversal occurs during the formation of the predominant buckling mode so that the strain-hardening or tangent modulus governs the bending reaction (the strain-hardening property is crucial to the theory). Predicted and experimental wavelengths are in reasonable agreement.

In this paper an alternative theory is postulated, again for rigid–plastic materials, to include yielding in a biaxial state of stress (in [1] a ring is substituted for a cylindrical shell) as well as strain hardening. As will be shown, the bending reaction now consists of two parts, one part due to the biaxial stress state and the other due to strain hardening. The former bending moment, the "directional" moment, is shown to provide the primary contribution to the bending reaction in the shells of the experiments (6061-T6 aluminum alloy); this conclusion is based on the relative influences of the directional and hardening moments on the final buckled shape. The theory predicts wavelengths in agreement with experimental wavelengths.

A theory of this type, involving a biaxial plastic stress state with strain hardening was first formulated by Goodier [2] to explain plastic flow buckling of flat plates due to in-plane forces. In the special case of longitudinal impact of flat plates, predicted and experimental wavelengths were in agreement. Later, the theory was adapted by Florence and Goodier [3] to describe the axisymmetric plastic flow buckling of tubes caused by axial impact. Again, predicted and experimental wavelengths were in agreement.

* This research was sponsored by the United States Air Force through the Air Force Weapons Laboratory under contract AF29(601)-7215.

In the development of the theory, unperturbed motion is analyzed first. During this motion the cylinder remains perfectly circular as it decreases in radius until all the initial kinetic energy is dissipated as plastic work. Then, the flow buckling is treated as a perturbation of this motion due to imperfections in the otherwise uniform radial displacements and velocities. It is supposed that the strain rates associated with unperturbed motion dominate the strain rates introduced by the perturbations so that no strain-rate reversal occurs until the buckling is well developed. In other words, stress states always remain on the current yield surface and have associated nonzero strain-rate vectors as outward normals. To keep the theory simple, the strain-hardening portion of the stress–strain curve from simple tensile tests is approximated by a straight line. Due to interest in moderately large deformations and corresponding high imploding velocities, elastic strains are neglected. Also, the material is regarded as incompressible and assumed to possess a stress–strain curve insensitive to strain rate. With these assumptions and suitable linearizations of equations, the solution, which is the shape of the shell at any time, is represented by the Fourier series (in angular coordinate θ) for the imperfection but with the amplitude of each harmonic amplified or weighted. The distribution of the amplification function with the harmonic number is characteristic for problems of this type [1–3] and exhibits a peak, meaning that certain harmonics are preferred. It is reasonable to choose the value of n at which the amplification function is a maximum to determine the predominant harmonic and hence the predicted wavelength.

The amplification function increases with time. Thus the maximum value occurs when motion ceases and, by definition, at the preferred mode. From the variation of the maximum value with the applied impulse a buckling criterion is derived which is essentially in agreement with that derived by Anderson and Lindberg [4].

THEORY OF PLASTIC CYLINDRICAL SHELLS

As shown in Fig. 1, x, θ, and z represent the longitudinal, circumferential, and radial coordinates, z being measured outwards from the cylindrical midsurface of radius a. The

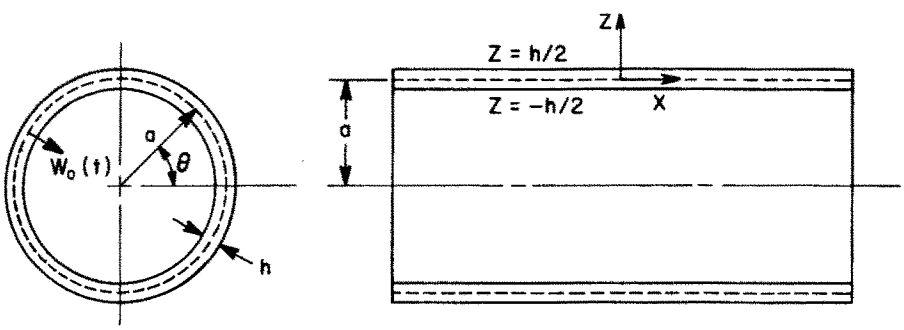

FIG. 1. Cylindrical shell—coordinates and dimensions.

thickness is h so z lies in the range $-h/2 \leq z \leq h/2$. With the corresponding components of strain rate denoted by $\dot{\varepsilon}_x$, $\dot{\varepsilon}_\theta$, and $\dot{\varepsilon}_z$ (dots denote time differentiation) the incompressibility condition is

$$\dot{\varepsilon}_x + \dot{\varepsilon}_\theta + \dot{\varepsilon}_z = 0 \tag{1}$$

The generalized strain rate $\dot{\varepsilon}$ and the generalized stress σ are defined by [5a]

$$\dot{\varepsilon}^2 = 2(\dot{\varepsilon}_x^2 + \dot{\varepsilon}_\theta^2 + \dot{\varepsilon}_z^2)/3 \tag{2}$$

and

$$\sigma^2 = 3(\sigma_x'^2 + \sigma_\theta'^2 + \sigma_z'^2)/2 \tag{3}$$

where σ_x', σ_θ', and σ_z' are the deviatoric stress components related to the actual stress components σ_x, σ_θ, and σ_z by

$$\sigma_x' = \sigma_x + p, \qquad \sigma_\theta' = \sigma_\theta + p, \qquad \sigma_z' = \sigma_z + p \tag{4}$$

with $p = -(\sigma_x + \sigma_\theta + \sigma_z)/3$. With the usual assumption of shell theory that the stress component perpendicular to the midsurface is negligible, setting $\sigma_z = 0$ in (4) gives

$$\sigma_x = 2\sigma_x' + \sigma_\theta', \qquad \sigma_\theta = 2\sigma_\theta' + \sigma_x'. \tag{5}$$

Introducing the Lévy–Mises flow law of incremental plasticity [5b]

$$\dot{\varepsilon}_x/\sigma_x' = \dot{\varepsilon}_\theta/\sigma_\theta' = \dot{\varepsilon}_z/\sigma_z' = \lambda \tag{6}$$

where λ is the proportionality factor [by (2), (3), and (6), $\lambda = 3\dot{\varepsilon}/2\sigma$], allows (5) to be written as

$$\sigma_x = 2(2\dot{\varepsilon}_x + \dot{\varepsilon}_\theta)\sigma/3\dot{\varepsilon}, \qquad \sigma_\theta = 2(2\dot{\varepsilon}_\theta + \dot{\varepsilon}_x)\sigma/3\dot{\varepsilon}. \tag{7}$$

With the assumption of linear strain hardening, the generalized stress and strain rates are related by $\dot{\sigma} = E_h\dot{\varepsilon}$ and hence

$$\sigma = \sigma_0 + E_h\varepsilon \tag{8}$$

where E_h is the slope of the line approximating the actual strain hardening portion of the stress–strain curve from a simple tension or compression test and σ_0 is simply the yield stress in such tests; σ_0 is the intitial value of the generalized stress which fixes the initial size of the von Mises yield ellipse in the σ_x, σ_θ plane.

THE UNPERTURBED MOTION

Let the current inward displacement of a uniform shell caused by a uniform impulse be $w_0(t)$. The circumferential component of strain rate is then

$$\dot{\varepsilon}_\theta = -(1 - z/a)(\dot{w}_0/a). \tag{9}$$

For sufficiently short shells with no axial restraints, axial extension occurs freely during motion there being no longitudinal component of membrane force at the ends and negligible longitudinal inertia. Thus the longitudinal stress component at the midsurface is taken to be zero. Setting $\sigma_x = \sigma_z = 0$ in (3) and (4) gives $\sigma_\theta = -\sigma$, $p = \sigma/3$, $\sigma_x' = \sigma_z' = \sigma/3$, and $\sigma_\theta' = -2\sigma/3$ at the midsurface. Hence, by (6), $\dot{\varepsilon}_x = -\dot{\varepsilon}_\theta/2 = \dot{\varepsilon}_z$ which, together with midsurface value $\dot{\varepsilon}_\theta = -\dot{w}_0/a$ from (9), leads to $\dot{\varepsilon}_x = \dot{\varepsilon}_z = \dot{w}_0/2a$ at the midsurface.

Based on the experimental observation that the generators of the cylindrical shells remain straight except in a narrow region near each end where the shells are flared outwards slightly, plane sections perpendicular to the axis are assumed to remain plane. This is equivalent to taking $\dot{\varepsilon}_x = \dot{w}_0/2a$ at all fibers or for all z. Combining this result with the

incompressibility condition (1) and the circumferential strain rate (9) gives

$$\dot{\varepsilon}_x = \dot{w}_0/2a, \qquad \dot{\varepsilon}_\theta = -(1-z/a)(\dot{w}_0/a), \qquad \dot{\varepsilon}_z = (1/2-z/a)(\dot{w}_0/a). \tag{10}$$

Substituting (10) into (2) gives $\dot{\varepsilon}^2 = (1-2z/a+4z^2/3a^2)(\dot{w}_0/a)$ which, since $(z/a)^2$ is assumed small, allows the following approximation for the generalized strain rate

$$\dot{\varepsilon} = (1-z/a)(\dot{w}_0/a). \tag{11}$$

Substituting (10) and (11) into (7) and neglecting powers of (z/a) higher than one leads to the stress formulas

$$\sigma_x = (2z/3a)\sigma, \qquad \sigma_\theta = -(1-z/3a)\sigma \tag{12}$$

and hence, by (8) and (11), the generalized stress is

$$\sigma = \sigma_0 + E_h(w_0/a)(1-z/a). \tag{13}$$

For notational convenience let σ^0 be the current generalized stress at the midsurface. Then, by (13),

$$\sigma^0 = \sigma_0 + E_h(w_0/a) \tag{14}$$

and after neglecting powers of (z/a) higher than one, (12) becomes

$$\begin{aligned} \sigma_x &= (2z/3a)\sigma^0 \\ \sigma_\theta &= -\sigma^0 + (z/3a)(\sigma_0 + 4E_h w_0/a). \end{aligned} \tag{15}$$

Figure 2 shows four yield ellipses in σ_x, σ_θ space. The inside ellipse shown dashed is the initial ellipse which applies to each fiber and its size is governed by the stress σ_0. The

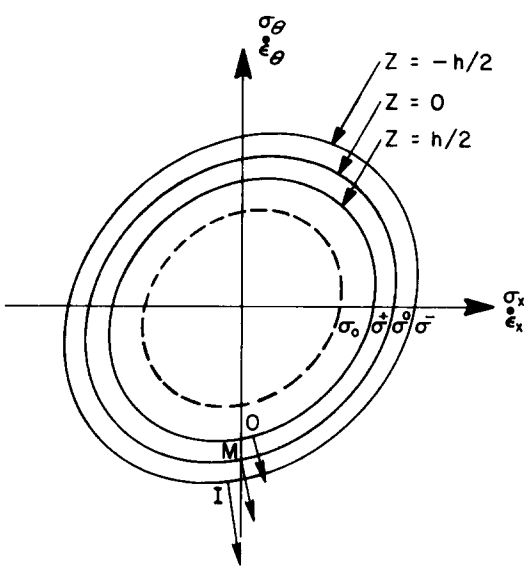

FIG. 2. Yield ellipses—plastic regimes for outer, middle, and inner fibers.

other three ellipses are current ellipses applicable to inner, middle, and outer fibers ($z = -h/2, 0, h/2$) with sizes governed by the stresses

$$\sigma^- = \sigma_0 + E_h(w_0/a)(1 + h/2a), \qquad \sigma^0 = \sigma_0 + E_h(w_0/a),$$

and

$$\sigma^+ = \sigma_0 + E_h(w_0/a)(1 - h/2a),$$

according to (13). Stresses at the inner, middle, and outer fibers, given by (15), are represented by the points I, M, and O; the strain rates, given by (10), are represented by the vectors at these stress points drawn perpendicular to the appropriate yield surface and these vectors have the same $\dot{\varepsilon}_x$ component, in accordance with (10).

With the membrane force and bending moment notation of Fig. 3(a) stress formulas (15) give

$$M_x = \int_{-h/2}^{h/2} \sigma_x z \, dz = (h^3/18a)\sigma^0$$
$$M_\theta = \int_{-h/2}^{h/2} \sigma_\theta z \, dz = (h^3/36a)(\sigma^0 + 3E_h w_0/a) \tag{16}$$

$$N_x = 0, \qquad N_\theta = -\sigma^0 h. \tag{17}$$

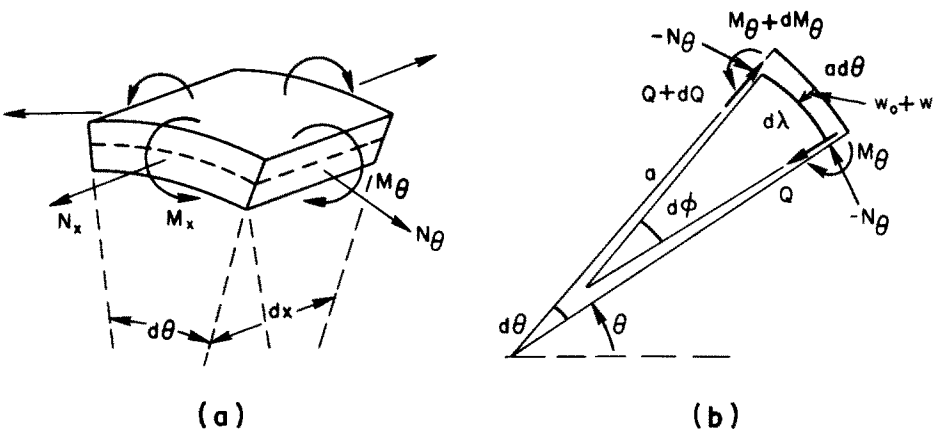

FIG. 3. Shell element—notation.

It is assumed that the lack of longitudinal bending moment M_x at each end of the shell affects the theory only in the narrow end regions where experiments show flaring.

The equation of motion of an element of shell subtending an angle $d\theta$ and of unit axial length is

$$N_\theta = a\rho h\ddot{w}_0. \tag{18}$$

Since $N_\theta = -\sigma^0 h$, where σ^0 is given by (14), equation (18) becomes

$$\dot{w}_0 + (c_h/a)^2 w_0 = -\sigma_0/a\rho \tag{19}$$

where $c_h^2 = E_h/\rho$. The solution of (19) with the initial conditions $w_0(0) = 0$ and $\dot{w}(0) = V_0$ is

$$w_0 = V_0(a/c_h)\sin(c_h t/a) - (\sigma_0 a/E_h)[1-\cos(c_h t/a)]. \tag{20}$$

Later, as a simplification of the theory the circumferential membrane force is approximated by $N_\theta = -\sigma_0 h$ resulting in a velocity $\dot{w}_0$ which decreases linearly with time.

THE PERTURBED MOTION

Let the additional inward radial deflection due to imperfections be $w(\theta, t)$ so that the total deflection is $w_0 + w$. Plane sections through the generators are assumed to remain plane and perpendicular to the midsurface.

The curvature of the deformed shell (Fig. 3b) is

$$\partial\varphi/\partial\lambda = \varkappa = 1/a + (w_0+w)/a^2 + w''/a^2 \tag{21}$$

where primes denote partial differentiation with respect to θ. Hence, by (21),

$$\dot{\varepsilon}_\theta = -(1-z/a)(w_0+w)^{\cdot}/a + (z/a^2)\dot{w}'' \tag{22}$$

which at the midsurface gives $\dot{\varepsilon}_\theta = -(w_0+w)^{\cdot}/a$. Employing the same assumptions and procedure for determining the strain rates (10) of the unperturbed motion, leads to

$$\begin{aligned}
\dot{\varepsilon}_x &= (w_0+w)^{\cdot}/2a \\
\dot{\varepsilon}_\theta &= -(1-z/a)(w_0+w)^{\cdot}/a + (z/a^2)\dot{w}'' \\
\dot{\varepsilon}_z &= (\tfrac{1}{2}-z/a)(w_0+w)^{\cdot}/a - (z/a^2)\dot{w}''.
\end{aligned} \tag{23}$$

In the results which follow, terms with powers of z/a higher than one and terms with products of perturbation quantities are neglected. Thus, by substituting (23) into (2), the generalized strain rate is found to be approximately

$$\dot{\varepsilon} = (w_0+w)^{\cdot}/a - (z/a)(w_0+w+w'')^{\cdot}. \tag{24}$$

Integration of (24) gives the generalized strain

$$\varepsilon = w_0/a + w/a - \bar{w}/a - (z/a)[w_0 + (w-\bar{w}) + (w-\bar{w})'']/a \tag{25}$$

where $\bar{w} = w(\theta, 0)$ is the initial value of the displacement perturbation. Substituting (25) into the strain hardening law (8) gives for the generalized stress

$$\sigma = \sigma^0 + E_h(w-\bar{w})/a - E_h(z/a)[w_0 + (w-\bar{w}) + (w-\bar{w})'']/a. \tag{26}$$

The stress formulas (7), with the strain rates $\dot{\varepsilon}_x$ and $\dot{\varepsilon}_\theta$ of (23), a two-term binomial approximation of $(\dot{\varepsilon})^{-1}$ from (24), and the generalized stress (26), become

$$\begin{aligned}
\sigma_x &= (2z/3a)[\sigma^0(1+\dot{w}''/\dot{w}_0) + E_h(w-\bar{w})/a] \\
\sigma_\theta &= -[\sigma^0 + E_h(w-\bar{w})/a] + (z/3a)[\sigma^0(1+\dot{w}''/\dot{w}^0) \\
&\quad + E_h\{3w_0 + 4(w-\bar{w}) + 3(w-\bar{w})''\}/a].
\end{aligned} \tag{27}$$

The stress distribution (27) has the following resultant membrane forces and bending moments.

$$N_x = 0, \qquad N_\theta = -[\sigma^0 + E_h(w-\bar{w})/a]h$$
$$M_x = [\sigma^0(1+\dot{w}''/\dot{w}_0) + E_h(w-\bar{w})/a](h^3/18a) \tag{28}$$
$$M_\theta = [\sigma^0(1+\dot{w}''/\dot{w}_0) + E_h\{3w_0 + 4(w-\bar{w}) + 3(w-\bar{w})''\}/a](h^3/36a).$$

The expression for the circumferential bending moment M_θ, which is the reaction moment in the buckling process, comprises two groups of terms. With the approximation $\sigma^0 \approx \sigma_0$ to be made later, the first group arises because of the dependence upon z of the plastic regime point on the current yield ellipse. This point, which determines the stress σ_θ, depends upon z even without strain hardening (stationary ellipse for rigid–perfectly plastic material) and results in a bending moment; from (28) this moment is $\sigma_0(1+\dot{w}''/\dot{w}_0) \times (h^3/36a)$. For a ring [1], setting $E_h = 0$ gives no reactive moment. This contribution is called here the directional moment and its existence depends upon yielding in a biaxial stress state. The second group is due entirely to strain hardening. A similar partitioning of bending moments exists in a plate [2].

THE GOVERNING EQUATION

With the aid of Fig. 3(b), which shows a unit element of shell with its attendant forces and moments, the following equations of motion or equilibrium can be derived:

$$Q = \frac{\partial M_\theta}{\partial \lambda}, \qquad \frac{\partial Q}{\partial \lambda} - N_\theta \frac{\partial \varphi}{\partial \lambda} = -\rho h \frac{\partial^2}{\partial t^2}(w_0 + w)$$

where the current element is $d\lambda$ subtending an angle $d\varphi$; its change in length is neglected so that $d\lambda = a\,d\theta$. The curvature $\varkappa = \partial\varphi/\partial\lambda$ is given by (21). Eliminating Q and φ leads to

$$M_\theta''/a^2 - N_\theta[1/a + (w_0+w)/a^2 + w''/a^2] + \rho h(w_0+w)^{\cdot\cdot} = 0. \tag{29}$$

Three approximations are now made to simplify (29). The hoop membrane force N_θ and the curvature are approximated by

$$N_\theta = -\sigma_0 h \quad \text{and} \quad \varkappa = 1/a + w''/a^2 \tag{30}$$

and thirdly, the term $4(w-\bar{w})$ in M_θ is neglected in comparison with the term $3(w-\bar{w})''$. Thus, after using (18) and setting $\sigma^0 = \sigma_0$ in (28), (29) becomes

$$[\sigma_0\dot{w}''/\dot{w}_0 + 3(E_h/a)(w-\bar{w})'']''(h^2/36a^3) + (\sigma_0/a^2)w'' + \rho\ddot{w} = 0. \tag{31}$$

The three terms, in order, represent effects of circumferential bending (directional plus hardening), circumferential membrane thrust, and inertia. By letting the radius become infinitely large and by replacing the imposed unperturbed strain rate $\dot{\varepsilon}_\theta = \dot{w}_0/a$ by its counterpart V_0/L in the longitudinal impact of a flat plate on length L, the corresponding plate equation [2] is obtained:

$$(\sigma_0 h^2 L/36V_0)\dot{w}'''' + (E_h h^2/12)(w-\bar{w})'''' + \sigma_0 w'' + \rho\ddot{w} = 0.$$

Introducing the dimensionless variables

$$u = w/a, \qquad \bar{u} = \bar{w}/a, \qquad u_0 = w_0/a, \qquad \tau = V_0 t/2a$$
$$\tau_f = \rho V_0^2/2\sigma_0, \qquad \alpha^2 = h^2/12a^2, \qquad \beta = E_h/\sigma_0 \tag{32}$$

(31) becomes

$$[\dot{u}''/\dot{u}_0 + 3\beta(u-\bar{u})'']''(\alpha^2/3) + u'' + (\tau_f/2)\ddot{u} = 0 \tag{33}$$

where now the dots denote differentiation with respect to τ.

SOLUTION IN TERMS OF BESSEL FUNCTIONS

As an approximation to the unperturbed motion (18) is replaced by $\sigma_0 = -a\rho\ddot{w}_0$ which in terms of the dimensionless variables (32) is $\ddot{u}_0 = -2/\tau_f$. With the initial conditions $u_0 = 0$ and $\dot{u}_0 = 2$ the dimensionless velocity is therefore $\dot{u}_0(\tau) = 2(1-\tau/\tau_f)$. Note that τ_f is not only the dimensionless time when motion ceases but is also the final maximum circumferential strain at the midsurface, i.e., $u_0(\tau_f) = \tau_f$. It is convenient to introduce one further dimensionless variable

$$\xi = 1-\tau/\tau_f, \qquad 0 \le \xi \le 1 \tag{34}$$

so that $\dot{u}_0 = 2\xi$ and (33) becomes

$$\ddot{u} + 2\tau_f u'' - \alpha^2[\dot{u}''/3\xi - 2\tau_f\beta(u-\bar{u})'']'' = 0 \tag{35}$$

where now the dots denote differentiation with respect to ξ.

General displacement perturbations are represented by the sum of a Fourier series in $\sin n\theta$ and $\cos n\theta$ but, since the differential equation governing the time variation of the coefficients $u_n(\xi)$ for the cosine series is the same as that for the sine series, only the following displacement perturbation is considered

$$u(\theta, \xi) = \sum_1^\infty u_n(\xi) \sin n\theta \tag{36}$$

having as initial displacement imperfections

$$\bar{u}(\theta, 1) = \sum_1^\infty a_n \sin n\theta. \tag{37}$$

By substituting (36) and (37) into (35), the differential equation for each amplitude u_n is

$$\ddot{u}_n - Q_n\dot{u}_n/\xi - R_n^2 u_n = S_n a_n \tag{38}$$

where

$$Q_n = \alpha^2 n^4/3, \qquad R_n^2 = 2\tau_f n^2(1-\alpha^2\beta n^2), \qquad S_n = 2\tau_f\alpha^2\beta n^4.$$

A representation of the initial velocity imperfections in the form

$$V = V_0\left(1 + \sum_1^\infty b_n \sin n\theta\right) \tag{39}$$

along with (37) for the initial displacement imperfections means that the coefficients u_n in (38) must satisfy the initial conditions

$$u_n(1) = a_n, \qquad \dot{u}_n(1) = -2\tau_f b_n. \tag{40}$$

Thus the solution of (38) with $R_n^2 > 0$ and subject to conditions (40) is

$$u_n(\xi) = A_n(\xi)a_n + B_n(\xi)b_n \tag{41}$$

where

$$\begin{aligned} A_n(\xi) &= \xi^\nu[I_\nu(R_n\xi)K_{\nu-1}(R_n) + K_\nu(R_n\xi)I_{\nu-1}(R_n)](R_n + S_n/R_n) - S_n/R_n^2 \\ B_n(\xi) &= 2\tau_f\xi^\nu[-I_\nu(R_n\xi)K_\nu(R_n) + K_\nu(R_n\xi)I_\nu(R_n)] \end{aligned} \tag{42}$$

I_ν and K_ν being modified Bessel functions of the first and second kinds of order $\nu = (1+Q_n)/2$. The relations (41) and (42) show that the current mode coefficients u_n equal the initial imperfection coefficients a_n and b_n multiplied by the respective amplification functions A_n and B_n. For the case of $R_n^2 < 0$ expressions similar to (42) arise but involving J_ν and Y_ν, Bessel functions of the first and second kinds; the solution is therefore of a damped oscillatory nature with $\xi^\nu J_\nu$ and $\xi^\nu Y_\nu$ approaching zero as ξ approaches zero (i.e., as motion terminates). Thus the growth of modes is confined to the case $R_n^2 > 0$ or $n^2 < 1/\alpha^2\beta$. This transition is analogous to that of [1] (which has only strain hardening moments) where hyperbolic and trigonometric functions occur instead of Bessel functions.

For general ξ ($0 \le \xi \le 1$) it is easier to solve (38) by numerical integration than by (42). However, for the terminal motion ($\xi \to 0$) an asymptotic form of (42) yields useful formulas.

THE AMPLIFICATION FUNCTIONS

In order to discuss further the nature of the amplification functions A_n and B_n one of the shells of the experiments is considered. The relevant data are

$$a = 1{\cdot}5\text{ in.}, \qquad h = 0{\cdot}065\text{ in.}, \qquad \rho = 2{\cdot}7\text{ g/cm}^3$$

$$\sigma_0 = 44 \times 10^3\text{ lb/in}^2, \qquad E_h = 0{\cdot}13 \times 10^6\text{ lb/in}^2$$

giving $a/h \approx 23$ and $\beta \approx 3$. Only modes with $n < 1/\alpha\beta^{\frac{1}{2}} = 46$ are amplified. For a range of values of n, for intervals of ξ of 0·2, and for an applied impulse of 8000 taps,* Figures 4(a) and 4(b) show the functions $A_n(\xi)$ and $B_n(\xi)$ resulting from the numerical integration of equation (38). The curves show the development of the amplification spectra, exhibiting a strong preference for a narrow band of harmonics. It is reasonable to select the most amplified harmonic to represent the final mode of buckling. The variation with ξ of the preferred harmonic is shown by the dashed lines in Fig. 4. Note that after $\tau = 0{\cdot}6\tau_f$ ($\xi = 0{\cdot}4$) the values of n at the maxima of $A_n(\xi)$ and $B_n(\xi)$ do not change significantly. At $\tau = \tau_f$ the preferred mode numbers stemming from initial displacement and velocity imperfections are 15 and 13. The theoretical curves in Fig. 4 are typical of all the shell experiments.

A measure of the amplitude of buckling of a cylindrical shell can be obtained from the variations of the maximum values of $A_n(0)$ and $B_n(0)$ (values at $\xi = 0$ or $\tau = \tau_f$) with the impulse $I = \rho h V_0$. For the shell being considered such variations are shown in Fig. 5, the preferred modes also being given along the curves. The rapid increase of $A_n(0)$ and $B_n(0)$

* 1 tap = 1 dyn-sec/cm^2.

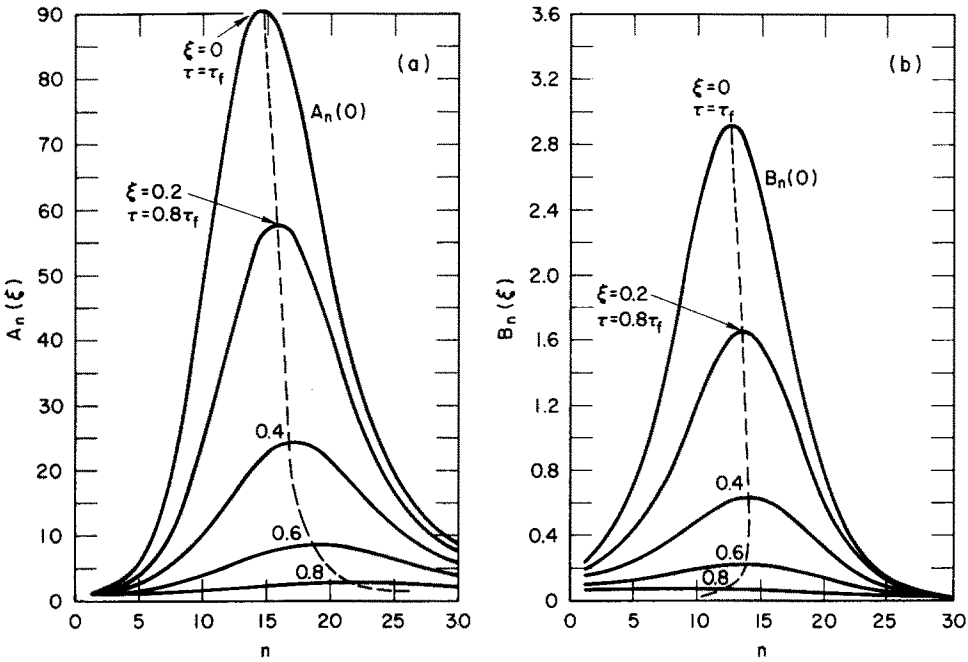

FIG. 4. Spectra of amplification factors: (a), displacement imperfections; (b), velocity imperfections.
(6061-T6 Aluminum, $a/h = 22{\cdot}6$, $I = 8000$ taps)

with impulse suggests that a buckling criterion based on a loosely specified magnification of the initial imperfections may be used. From Fig. 5 it can be seen that the values of $A_n(0)$ are greater than those of $B_n(0)$ by a factor of about 25. However, choosing reasonable radius imperfections of about one-hundredth of the wall thickness and velocity imperfections of about one percent of the average initial velocity, magnifications of 50 and 2 for $A_n(0)$ and $B_n(0)$ result in wrinkles of amplitudes $0{\cdot}5h$ and $0{\cdot}46h$.

ASYMPTOTIC SOLUTION FOR TERMINAL MOTION

Assuming no strain-rate reversal during the entire inward motion (of duration τ_f), relatively simple expressions for the final values of the amplification functions can be derived from (42).

As $\xi \to 0$, $\xi^\nu I_\nu(R_n\xi) \to 0$ and $\xi^\nu K_\nu(R_n\xi) \to 2^{\nu-1}\Gamma(\nu)/R_n^\nu$ where $\Gamma(\nu)$ is the gamma function. Also, for R_n sufficiently greater than ν, $I_\nu(R_n) \sim e^{R_n}/(2\pi R_n)^{\frac{1}{2}}$. This asymptotic representation is shown later to be satisfactory for the shells of the experiments. Finally, it is assumed that $S_n/R_n^2 = \alpha^2\beta n^2 \ll 1$. With these approximations the amplification factors (42), evaluated at $\xi = 0$, become

$$\begin{aligned} A_n(0) &= 2^{\nu-1}\Gamma(\nu)\, e^{R_n}/[(2\pi)^{\frac{1}{2}}R_n^{\nu-\frac{1}{2}}] \\ B_n(0) &= \tau_f 2^\nu \Gamma(\nu)\, e^{R_n}/[(2\pi)^{\frac{1}{2}}R_n^{\nu+\frac{1}{2}}]. \end{aligned} \tag{43}$$

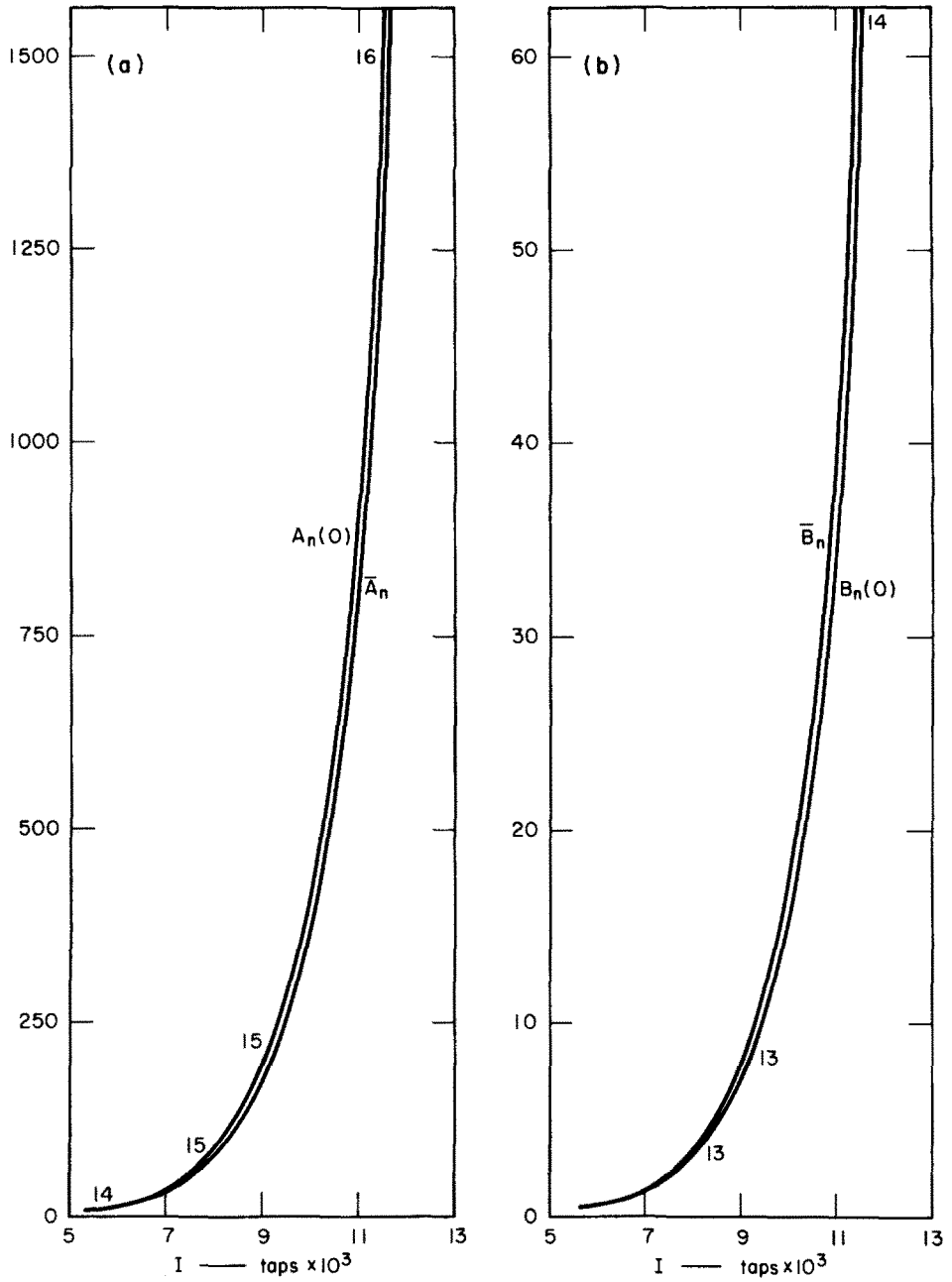

FIG. 5. Impulse vs. amplification curves: (a), displacement imperfections; (b), velocity imperfections.
(6061-T6 Aluminum, $a/h = 22{\cdot}6$, $a = 1{\cdot}47$ in.)

By regarding $A_n(0)$ and $B_n(0)$ as functions of the continuous variable n the maxima are found to be at values of n (closest integer n is the preferred mode in each case), which are solutions of the equations

$$R_n - 2Q_n \ln(R_n/2) - (Q_n/2 - 2Q_n\psi) = 0 \tag{44}$$

$$R_n - 2Q_n \ln(R_n/2) - (1 + Q_n/2 - 2Q_n\psi) = 0 \tag{45}$$

where ψ is the ψ-function [6] defined by $(d/dv) \ln \Gamma(v)$. In deriving (44) and (45) the approximation $\alpha^2\beta n^2 \ll 1$ is used, giving $R_n^2 \approx 2\tau_f n^2$.

To justify the above and further approximations the shell data ($a/h = 23$, $\beta = 3$) of the previous section is used. Firstly, only modes with $n < 1/\alpha\beta^{\frac{1}{4}} = 46$ are amplified. Secondly, the thrust effect without the restraining directional moment effect is a maximum when R_n^2 is a maximum, i.e., when $n = 1/(2\alpha^2\beta)^{\frac{1}{4}} = 33$. At this value of n, $R_n^2 = 109$ (using a final strain of $\tau_f = \frac{1}{10}$), $R_n = 10{\cdot}5$, and $Q_n = 62$. Below this value of n, R_n^2 decreases as n^2 but Q_n decreases as n^4 indicating that the relative effects of directional moment and thrust are such that the most amplified mode is well below $n = 33$. Anticipating a theoretical prediction of a preferred number close to the experimental value of $n = 14$ the approximation $\alpha^2\beta n^2 \ll 1$ becomes $\alpha^2\beta n^2 = \frac{1}{11}$. For the lower modes, $Q_n < 1$ when $n < 12$; at $n = 12$, $Q_n = 1.1$, $R_n^2 = 29$, and $R_n = 5{\cdot}4$. As R_n is varied from 5 to 10 the ranges of Q_n from (44) and (45) are respectively 1·7 to 2·4 and 2·1 to 2·7 ($2Q_n\psi$ term neglected). These narrow ranges restrict the preferred mode predictions to $n = 13$ or 14 for displacement imperfections and to $n = 14$ or 15 for velocity imperfections. Although not exactly the solution of either (44) and (45) the approximation

$$Q_n = \alpha^2 n^4/3 = 2 \tag{46}$$

appears justifiable for the experimental shells. A consequence of (46) is that $v = \frac{3}{2}$ where $\Gamma(v)$ is close to a minimum and hence ψ is small; also R_n is sufficiently larger than v to permit the above asymptotic expression for $I_v(R_n)$. Using the approximation (46) in (43) gives for the maximum amplification functions the expressions

$$\bar{A}_n = e^{R_n}/2R_n \quad \text{and} \quad \bar{B}_n = \tau_f e^{R_n}/R_n^2 \quad \text{where} \quad R_n^2 \approx 2\tau_f n^2. \tag{47}$$

Formulas (47) describe curves similar to the $\xi = 0$ curves in Fig. 4 in the neighborhood of the peaks. The variations with impulse of the amplification functions determined by (47) are shown in Fig. 5 beside the corresponding curves obtained by numerical integration. For a given magnification, formulas (47) predict almost the same impulses as the $A_n(0)$ and $B_n(0)$ curves. In (47), note that the impulse I is related to the final strain τ_f by $\tau_f = \rho V_0^2/2\sigma_0 = I^2/2\rho\sigma_0 h^2$.

THRESHOLD IMPULSE

By equating the initial kinetic energy to the plastic work done in membrane compression it follows that $I = (2\tau_f\rho\sigma_0)^{\frac{1}{2}}h$. Using the approximate expression in (47) for R_n gives $(2\tau_f)^{\frac{1}{2}} = R_n/n$ where n is the preferred mode which, from (46), is $n = (72)^{\frac{1}{4}}(a/h)^{\frac{1}{2}}$. Thus the impulse formula becomes

$$I = [R_n/(72)^{\frac{1}{4}}]a(\rho\sigma_0)^{\frac{1}{2}}(h/a)^{\frac{1}{2}}. \tag{48}$$

Due to the steepness of the amplification vs. impulse curves (Fig. 5) above a certain range of impulse, theoretical impulses required to cause collapse of the shells can be estimated. This estimation is based on a value of amplification factor chosen to be on that part of the curve where small changes in impulse cause large changes in amplification. From (47), the value of R_n corresponding to a reasonable choice of amplification factor of $\bar{A}_n = 100$ is $R_n = 7{\cdot}3$ (a factor of $\bar{A}_n = 500$ gives $R_n \approx 9$, a relatively small increase of R_n). Using this

value of R_n in (48) gives

$$I = 2{\cdot}5\, a(\rho\sigma_0)^{\frac{1}{2}}(h/a)^{\frac{3}{2}} \tag{49}$$

which, apart from the numerical factor, has the same form as that derived by Anderson and Lindberg [4]. The collapse impulses of the shells by increasing thickness estimated by (49) are 7800, 11,200, and 13,800 taps and the final compressive membrane strains corresponding to $R_n = 7{\cdot}3$ are 14, 18, and 21 per cent.

According to the few experimental results presented here a suggested impulse formula where the amplitudes of the wrinkles are still a small fraction of the wall thickness, is that given in [4], namely.

$$I_T = 1{\cdot}3\, a(\rho\sigma_0)^{\frac{1}{2}}(h/a)^{\frac{3}{2}}. \tag{50}$$

(Formula (50) corresponds to $R_n = 3{\cdot}8$, $\bar{A}_n \approx 6{\cdot}0$, $\tau_f \approx 3{\cdot}8$, 4·8, and 5·6 per cent, $I_T = 4100$, 5800, and 7100 taps.) Formula (50) thus represents an experimental adjustment of the numerical coefficient of (49).

COMPARISON OF THEORY AND EXPERIMENT

Table 1 contains the main experimental data. Each shell was impulsively loaded using the experimental method described fully in [1]. Briefly, this method consists of enclosing the cylinder with an attenuator of neoprene foam, $\frac{1}{4}$-in. thick, and wrapping a uniform sheet of explosive, 15 mils thick, around the attenuator. The explosive sheet extends beyond the shell in the axial direction to form a conical "run-up" section. Upon detonating the explosive at the apex a ring of high pressure at the detonation front runs up to the shell and traverses it at about 7·2 mm/μsec.

The impulses were obtained by measuring the velocities of aluminum disks having the same thicknesses as the shells. Neoprene foam, $\frac{1}{4}$-in. thick, again served as an attenuator so the explosive–attenuator–aluminum configuration conformed to the shell experiments. A double flash X-ray unit was used to measure the disk velocities.

Magnified shell profiles were drawn by rotating each wrinkled shell so that a radially oriented pointer bearing against the shell moves outwards and inwards. The pointer is an extension of the core of a linear differential transformer and movement activates a plotter. With this device many imperceptible buckles were magnified sufficiently to allow a count of the number of waves around the circumference. Profiles were taken at $\frac{1}{2}$-in. intervals along the shells and an average number of waves, to the nearest integer, recorded for each shell. These mode numbers were found to be highly reproducible and the averages are listed in Table 1.

One of the reasons for choosing 6061-T6 aluminum alloy is that it is insensitive to strain rate at room temperature [7]. It is possible to postulate a theory of dynamic plastic buckling on a strain-rate property alone [8]. Another reason for the choice is that the slope E_h of the straight line representing an approximation to the hardening portion of the stress–strain curve is small enough to allow the reasonable approximation of constant compressive membrane stress in the unperturbed motion. The large variation of E_h especially for small plastic strains has not been taken into account in the theory. A treatment of this problem can be found in [4]. A final reason for the choice is that it is a material of practical interest. The value of the yield stress σ_0 shown in Table 1 is defined here as the

TABLE 1. EXPERIMENTAL AND THEORETICAL RESULTS

No. of cylinders	Radius, a (in.)	Thickness, h (in.)	a/h	Length (in.)	Mode Numbers				Experim. impulse (taps)*	Theoret. threshold impulse Eq. (50) (taps)	Final theoret. strain τ_f (%)	Final experim. strain ε_θ (%)	Experim. strain ratio $-\varepsilon_x/\varepsilon_\theta$
					Experiment	Theory							
						Eq. (44) Displacement imperfection	Eq. (45) Velocity imperfection	Eq. (46) $n = (72)^{\frac{1}{4}} \times (a/h)^{\frac{1}{2}}$					
3	1·468	0·065	22·6	1	15	14	13	14	6500	4100	3·8	9·4	0·43
3	1·468	0·065	22·6	2	15	14	13	14	6500	4100	3·8	9·4	0·37
2	1·468	0·065	22·6	4	16	14	13	14	6500	4100	3·8	9·4	0·26
1	1·468	0·065	22·6	8	19	14	13	14	6300	4100	3·8	9·4	0·10
1	1·468	0·065	22·6	12	20	14	13	14	6300	4100	3·8	9·4	0·04
3	1·459	0·083	17·6	1	14	13	12	12	6600	5800	4·8	6·4	0·48
3	1·459	0·083	17·6	2	15	13	12	12	6600	5800	4·8	6·4	0·38
2	1·459	0·083	17·6	4	15	13	12	12	6600	5800	4·8	6·4	0·31
3	1·453	0·095	15·3	1	11	12	11	11	6900	7100	5·6	5·3	0·45
3	1·453	0·095	15·3	2	12	12	11	11	6900	7100	5·6	5·3	0·31
2	1·453	0·095	15·3	4	12	12	11	11	6900	7100	5·6	5·3	0·31

Shell Data: 6061-T6 aluminum, outside diameter 3 in., average $E_h = 0{\cdot}13 \times 10^6$ lb/in^2 ($8{\cdot}85 \times 10^9$ dyn/cm^2), $\sigma_0 = 44{,}000$ lb/in^2 ($3{\cdot}0 \times 10^9$ dyn/cm^2), $\rho = 2{\cdot}7$ g/cm^3.
* 1 tap = 1 dyn-sec/cm^2.

ordinate of the point of intersection of the two straight lines representing the elastic and strain-hardening portions of the stress–strain diagram.

The theoretical preferred mode numbers which are the solutions of equations (44) and (45) and are approximated by the simple formula (46) can be seen in Table 1 to be in agreement with the experimental numbers except for the 8- and 12-in. long shells. This is attributed to the difference between the original assumption equivalent to $\varepsilon_x/\varepsilon_\theta = -\frac{1}{2}$ and the final measured values of this ratio. Table 1 shows that the approximation is reasonable for 1-in. long shells but becomes progressively worse the longer the shell. Thus the theory is limited to short shells.

No attempt was made in this experimental program to obtain threshold impulses to produce amplitude of buckles which are small fractions of wall thicknesses. The impulses are all about the same level producing amplitudes which are mostly less than about $h/3$, $h/5$, and $h/8$ for shell thicknesses of 0·065, 0·083, and 0·095 in. The thickest shell conforms somewhat with the above concept of threshold impulse and, as can be seen in Table 1, the theoretical impulse predicted by (50) is close to the experimental value. For the other two shell thicknesses the threshold impulses are below the experimental values as they should be.

The preferred mode numbers obtained by numerical integration of the governing equation (38), using the threshold impulses and displacement imperfections, are 13, 12, and 11 for $\beta = 0$ ($E_h = 0$) and 13, 11, and 10 for $\beta = 5$ so that over quite a wide range of E_h values (0–220,000 lb/in^2) the mode numbers are relatively unaffected. This insensitivity implies that for the shells in Table 1 the main contribution to the restoring moment comes from the direction moment, according to a theoretical model having a constant strain hardening modulus E_h. For values of β in the range $0 < \beta < 3$ the approximations $R_n = (2\tau_f)^{\frac{1}{2}} n(1-\alpha^2\beta n^2)^{\frac{1}{2}} \approx (2\tau_f)^{\frac{1}{2}} n(1-\alpha^2\beta n^2/2) \approx (2\tau_f)^{\frac{1}{2}} n$ are reasonable because $\alpha^2\beta n^2 = (h/a)\beta/2^{\frac{1}{2}}$ is small enough and thus the threshold impulses (50) are not significantly affected.

CONCLUSIONS

A theory has been postulated to explain the plastic flow buckling of short cylindrical shells subjected to uniform radially inward impulses. Formulas have been derived which predict mode numbers and threshold impulses in general agreement with experimental results. The results suggest that the theory applies to shells with lengths less than diameters.

In the theory, the plastic flow which takes place in a biaxial stress state gives rise to a directional moment contribution to the restoring moment in addition to the usual hardening moment. Based on the relative influence of these contributions on the predictions of preferred modes and threshold impulses for the short shells of the experiments, the directional moments have the primary effect. This conclusion does not necessarily apply to long shells nor to shells of material like 6061-T6 aluminum which have final plastic strains which are only a few times the elastic yield strain. It is expected that the longer the shell, the greater the relative contribution of the hardening moment; also the smaller the final plastic strain, the greater the relative contribution of the hardening moment (because of the larger average values of E_h and β).

Acknowledgements—The authors are indebted to Professor J. N. Goodier, Dr. G. R. Abrahamson, and Dr. H. E. Lindberg for fruitful discussions and to W. A. Zietzke for carrying out the experiments.

REFERENCES

[1] G. R. ABRAHAMSON and J. N. GOODIER, Dynamic plastic flow buckling of a cylindrical shell from uniform radial impulse, *Proc. 4th U.S. natn. Congr. appl. Mech.*, June 18, 1962, Vol. 2, pp. 939–950.
[2] J. N. GOODIER, Dynamic buckling of rectangular plates in sustained plastic compressive flow. *Proc. Symp. on Plasticity*, Cambridge University Engineering Laboratory, April 1968.
[3] A. L. FLORENCE and J. N. GOODIER, Dynamic plastic buckling of cylindrical shells in sustained axial compressive flow. *J. appl. Mech.* **35**, 80–86 (1968).
[4] D. L. ANDERSON and H. E. LINDBERG, Dynamic pulse buckling of cylindrical shells under transient lateral pressures. *AIAA Jnl* **6**, 589–597 (1968).
[5] R. HILL, *The Mathematical Theory of Plasticity*, Chapter II, (a) p. 30, (b) p. 38. Oxford University Press (1950).
[6] A. ERDÉLYI, *Higher Transcendental Functions*, Vol. I, p. 15. McGraw-Hill (1953).
[7] D. L. HOLT, S. G. BABCOCK, S. J. GREEN and C. J. MAIDEN, The strain-rate dependence of the flow stress in some aluminum alloys. *Trans. Am. Soc. mech. Engrs* **60**, No. 2 (1967).
[8] A. L. FLORENCE, Buckling of visco-plastic cylindrical shells due to impulsive loading. *AIAA Jnl* **6**, 532–537 (1968).

(*Received* 17 *November* 1967; *revised* 9 *February* 1968)

Абстракт—Предлагается теория выясняющая динамическое пластическое выпучивание коротких, цилиндрических оболочек, подверхенных радиально равномерным, внутренним импульсам. Выводятся формули, определяющие длины волн (или числа форм выпучивания) и импульсы порога, в общей сходимости с представленными экспериментальными результатами. Согласно этой теории, востанавливающей момент первоначально состоит из момента зависящего от направления, вызванного приведением оболочки в двухосное пластическое напряженное состсяние. Для практических используемых значений деформации при упрочнении добавка упорчнения к востанавливающему моменту является второстепенной. Эта заметка основанна на относительных влияниях для представленных форм выпучивания и импульсов порога.